

## Accuracy of plagioclase compositions from laboratory and Mars spacecraft thermal emission spectra

Keith A. Milam,<sup>1</sup> Harry Y. McSween Jr.,<sup>1</sup> Victoria E. Hamilton,<sup>2</sup> Jeffrey M. Moersch,<sup>1</sup> and Philip R. Christensen<sup>3</sup>

Received 28 March 2003; revised 14 November 2003; accepted 13 January 2004; published 7 April 2004.

[1] Plagioclase, the most abundant mineral in many terrestrial and Martian igneous rocks, exhibits a range of compositions that reflects changing conditions during crystallization. Thermal emission spectrometers (TES, THEMIS, and Mini-TES) on board Mars spacecraft provide a means of determining average plagioclase compositions directly. We demonstrate that spectrally modeled average plagioclase compositions in terrestrial basalts, andesites, and dacites correspond to measured values to within  $+10/-6$  An (molar  $[Ca/(Ca + Na)] \times 100$ ) of weighted average values and  $+13/-14$  An of normative compositions. Analyses of spectra from two-component plagioclase mixtures (varied by volume and composition) provide additional insight into potential effects of plagioclase zoning. Considering the variability in types of observed plagioclase zoning patterns in terrestrial volcanic rocks, normal zoning (calcic cores and sodic rims) cannot be assumed and thus cannot account for an apparent “sodic bias” seen in previous spectrally modeled compositions. This bias is better explained by higher abundances of sodic groundmass plagioclase relative to calcic phenocrysts. Deconvolution modeling of laboratory spectra of physical mixtures (convolved to various instrument resolutions) predicts that TES, THEMIS, and Mini-TES spectra may be used to extract plagioclase compositions to within  $+9/-12$  An,  $+11/-12$  An, and  $+8/12$  An (respectively) of measured values in coarse sand plagioclase mixtures, with  $1\sigma$  standard deviations of  $\pm 4$  An for laboratory, TES, and Mini-TES resolutions and  $\pm 6$  An for THEMIS resolution. *INDEX TERMS:* 5464 Planetology: Solid Surface Planets: Remote sensing; 6225 Planetology: Solar System Objects: Mars; 5494 Planetology: Solid Surface Planets: Instruments and techniques; 3672 Mineralogy and Petrology: Planetary mineralogy and petrology (5410); 1060 Geochemistry: Planetary geochemistry (5405, 5410, 5704, 5709, 6005, 6008); *KEYWORDS:* Gusev, MER rover, THEMIS, TES, MOLA, MOC

**Citation:** Milam, K. A., H. Y. McSween Jr., V. E. Hamilton, J. M. Moersch, and P. R. Christensen (2004), Accuracy of plagioclase compositions from laboratory and Mars spacecraft thermal emission spectra, *J. Geophys. Res.*, 109, E04001, doi:10.1029/2003JE002097.

### 1. Introduction

[2] Feldspars are the most common minerals in the terrestrial and Martian crusts. The application of thermal infrared (TIR) spectroscopy to Mars (the Thermal Emission Spectrometer (TES) [Christensen *et al.*, 1992, 2001] on Mars Global Surveyor, the Thermal Emission Imaging System (THEMIS) [Christensen *et al.*, 2004] on Mars Odyssey, and the Miniature Thermal Emission Spectrometers (Mini-TES) [Christensen *et al.*, 2003] on the Mars Exploration Rovers) offers a remote-sensing technique that

can directly identify feldspars. From the compositions and proportions of feldspar standards used in spectral deconvolution, it is also possible to estimate plagioclase compositions. Previous studies suggest that modeled plagioclase abundances from TIR spectra are reasonably accurate [Hamilton *et al.*, 1997; Hamilton and Christensen, 2000], but modeled compositions may be biased toward sodic compositions [Wyatt *et al.*, 2001].

[3] Plagioclase minerals are solid solutions of  $CaAl_2Si_2O_8$  (anorthite, An) and  $NaAlSi_3O_8$  (albite, Ab) end-members, containing minor (<10%)  $KAlSi_3O_8$  (orthoclase, Or). Volcanic rocks typically contain phenocrysts of calcic plagioclase, with smaller crystals of more sodic plagioclase in the groundmass. Commonly these grains are chemically zoned in complex patterns, reflecting growth under varying conditions as the magma cooled. Thus volcanic rocks are likely to contain plagioclase showing a range of compositions.

[4] Much is known about the spectral characteristics displayed by feldspars in the thermal infrared. TIR spectral studies of plagioclase feldspars and plagioclase-dominated

<sup>1</sup>Planetary Geosciences Institute, Department of Earth and Planetary Sciences, University of Tennessee, Knoxville, Tennessee, USA.

<sup>2</sup>Hawaii Institute of Geophysics and Planetology, University of Hawaii at Manoa, Honolulu, Hawaii, USA.

<sup>3</sup>Department of Geological Sciences, Arizona State University, Tempe, Arizona, USA.

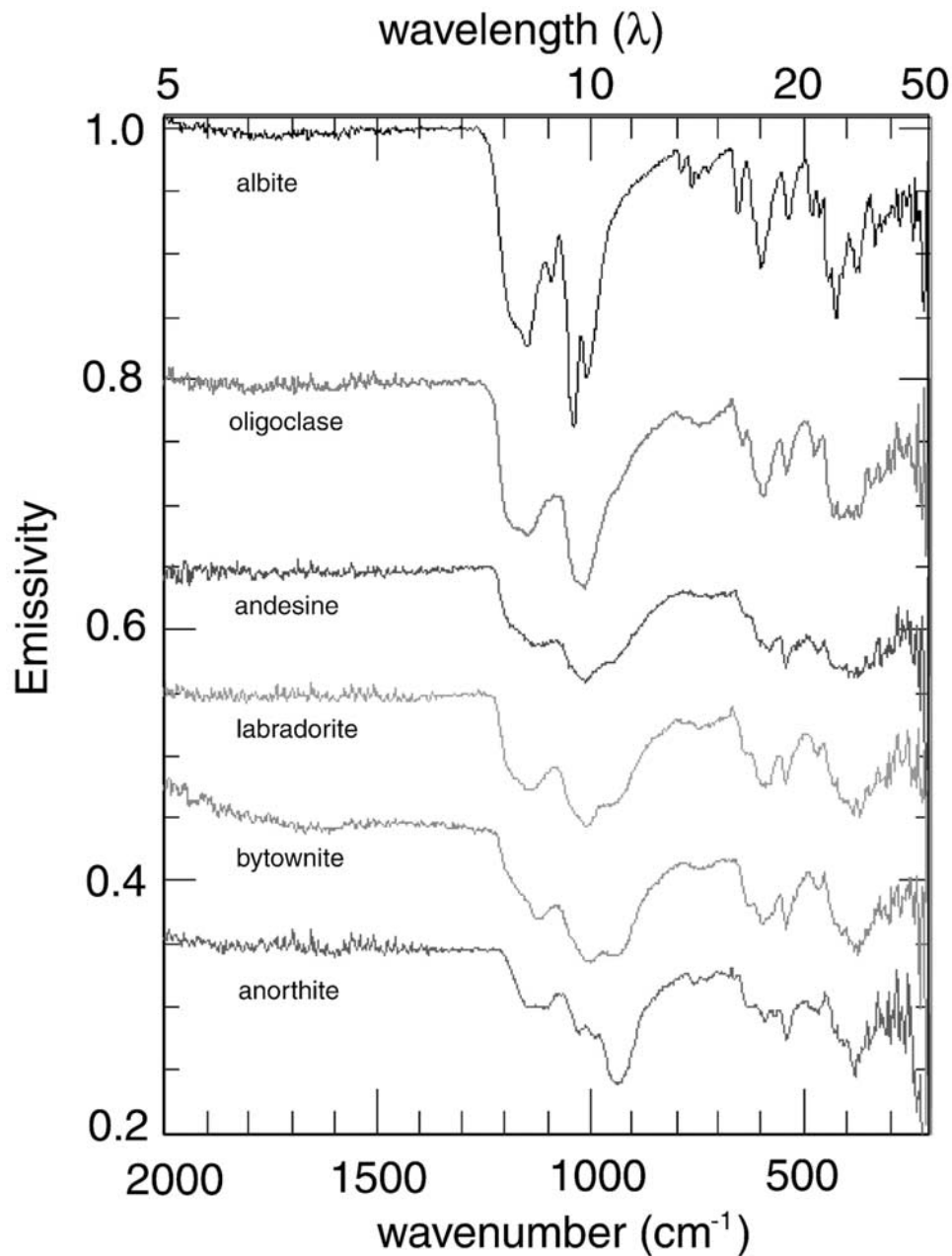


**Figure 1.** Emissivity spectra of solid solution plagioclase ranging from albite to anorthite. All spectra, except albite, are offset for clarity.

mafic igneous rocks have shown the extent to which plagioclase abundances can be derived. *Thomson and Salisbury* [1993] showed that modal abundances of minerals in mixtures (some involving feldspars) can be determined to within 5–12%. Later studies [*Feely and Christensen*, 1999; *Hamilton and Christensen*, 2000] agreed with this, showing that major mineral phases can be modeled to within 6–15 vol. % of measured abundances. *Feely and Christensen* [1999] showed that total feldspar abundances can be modeled to within 11 vol. %, while others have shown that plagioclase itself can be determined to within 5–10 volume % [*Hamilton et al.*, 1997; *Wyatt et al.*, 2001].

[5] Additional spectral studies have shown the extent to which plagioclase compositions can be modeled. *Nash and*

*Salisbury* [1991] demonstrated that plagioclase has distinct spectral signatures in the mid-IR (4–15  $\mu\text{m}$ ) region and that the shapes and positions of band features and the Christiansen Frequency (a prominent reflectivity minimum/emissivity maximum between  $\sim 7.7$ – $8.1 \mu\text{m}$ ) vary with changing solid solution, making it possible to determine plagioclase compositions using infrared spectra. A study covering an extended spectral range (1400–200  $\text{cm}^{-1}$ ) in the TIR by *Ruff* [1998] supported this conclusion by demonstrating that compositional and structural variations in plagioclase can be discerned by their distinctive spectral features. Plagioclase (compositions ranging from albite to anorthite) spectra are shown in Figure 1. The Christiansen Frequency shows a shift to higher wave numbers as plagioclase compositions

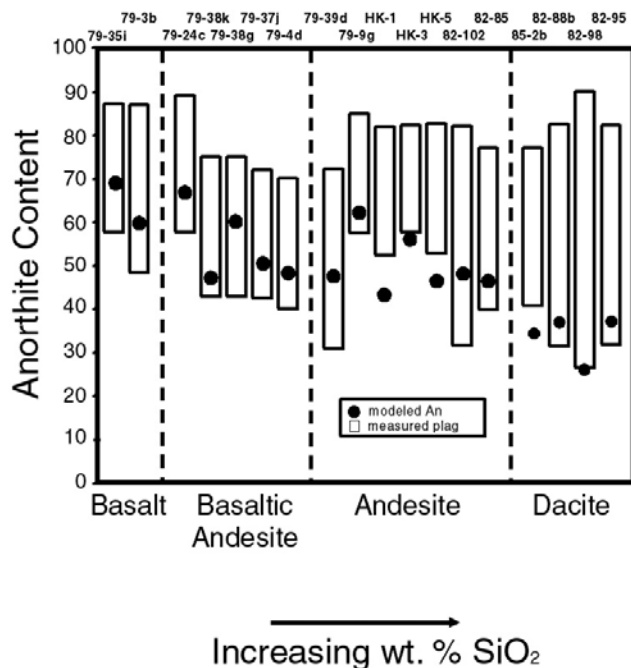


**Figure 2.** Comparison of spectrally modeled plagioclase compositions with measured plagioclase compositional ranges, after *Wyatt et al.* [2001]. Note that modeled values plot near the sodic ends of measured compositional ranges. Four modeled values lie outside the analyzed ranges.

change from albite to anorthite. Additional spectral features at 1200–900, 800–700, and 650–540  $\text{cm}^{-1}$  result from various Si, Al, and O stretching/bending modes in plagioclase [*Iiishi et al.*, 1971; *Ruff*, 1998]. Other spectral minima appear below 540  $\text{cm}^{-1}$  due primarily to cation-O stretching modes [*Iiishi et al.*, 1971; *Ruff*, 1998]. Work by *Hamilton and Christensen* [2000] suggested that plagioclase compositions could be derived to within 10–15 An using a linear deconvolution technique similar to that of *Ramsey and Christensen* [1998] developed by J. L. Bandfield.

[6] *Wyatt et al.* [2001] studied thermal emission spectra of terrestrial volcanic rocks ranging in composition from basalt to dacite and suggested that there may be a larger uncertainty in derived plagioclase compositions than previously thought. Plagioclase compositions in that study were modeled by normalizing percentages of the total plagioclase end-members used in the deconvolution to 100%, multiplying individual contributions by their respective anorthite contents, and summing the results [*Hamilton and Christensen*, 2000]. Anorthite content (the molar ratio of Ca/Ca + Na in solid-solution plagioclase  $\times$  100) for spectral library standards was determined from laboratory geochemical measurements [*Christensen et al.*, 2000]. Modeled An was then compared to measured plagioclase compositional ranges for each sample. Figure 2 shows that of the 18 rocks studied by *Wyatt et al.* [2001], 14 modeled compositions were within the reported plagioclase compositional ranges for each sample. However, all 14 modeled compositions were more sodic (i.e., lower An) than median values for the measured compositional ranges. The remaining 4 modeled compositions were also more Na-rich and outside measured

compositional ranges. This suggests that the linear deconvolution technique models plagioclase compositions as more sodic than median or measured ranges of plagioclase compositions. Here we use the term “sodic bias” to denote this potential modeling effect. *Wyatt et al.* [2001] suggested that the sodic bias resulted from a volumetric dominance of sodic groundmass and sodic rim material on normally zoned (calcic core, sodic rim) phenocrysts to the overall rock spectra. Because large uncertainties in determining average plagioclase compositions would limit petrogenetic interpretations of laboratory and Martian spectral data, we have studied the cause of the apparent sodic bias in further detail.

[7] First, we examine terrestrial volcanic rocks and focus on the mixing of phenocryst and groundmass plagioclase. We use laboratory geochemical and spectral analyses to address whether the assumption of sodic plagioclase in mesostasis and normal zoning in terrestrial volcanic rocks is correct, and if the apparent sodic bias is the result of volumetrically dominant sodic groundmass.

[8] Secondly, we assess the potential effects of plagioclase zoning on thermal emission spectra of volcanic rocks. Mixtures of pure plagioclase sands of varying composition and proportion are used to simulate zoning. TIR spectra are generally dominated by sand-size particles in Martian dark regions [*Christensen et al.*, 2001], and large zoned grains on Mars could be broken into roughly homogenous grains and mixed. Geochemical and spectral analyses of these mixtures were performed to determine whether plagioclase zoning itself produces a “sodic bias” to average measured values. Finally, we examine the applicability of laboratory results to TES, THEMIS, and Mini-TES data by resampling laboratory emissivity spectra to that of each instrument, performing deconvolutions of the spectra, estimating plagioclase compositions, and comparing our results to the known compositions.

## 2. Experimental and Analytical Techniques

### 2.1. Rocks: Phenocrysts Versus Groundmass

#### 2.1.1. Sample Acquisition and Preparation

[9] Volcanic rocks, ranging from basalt to dacite (Figure 3), were selected from a variety of tectonic settings (Table 1). Most specimens (except 79-35i) contained plagioclase as both phenocrysts and groundmass (Figure 4). Several

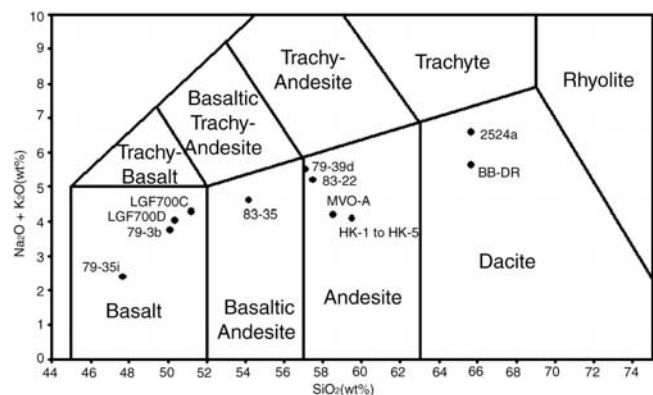


**Figure 3.** Volcanic rock classification for rock samples (Table 1) in part 1.

**Table 1.** Sample Sources and Bulk Chemistry for Rocks in Part 1

| Sample                    | Source <sup>a</sup> | Locality                                 | SiO <sub>2</sub> | Al <sub>2</sub> O <sub>3</sub> | Fe <sub>2</sub> O <sub>3</sub> | MgO   | CaO   | Na <sub>2</sub> O | K <sub>2</sub> O | TiO <sub>2</sub> | P <sub>2</sub> O <sub>5</sub> | MnO  | LOI  | Total  |
|---------------------------|---------------------|--|------------------|--------------------------------|--------------------------------|-------|-------|-------------------|------------------|------------------|-------------------------------|------|------|--------|
| <i>Basalts</i>            |                     |  |                  |                                |                                |       |       |                   |                  |                  |                               |      |      |        |
| 79-35i                    | 1, 2                | Medicine Lake Highlands, CA              | 47.68            | 17.74                          | 9.72                           | 9.35  | 11.74 | 2.30              | 0.09             | 0.71             | 0.06                          | 0.16 |      | 99.55  |
| 79-3b                     | 1, 2                | Medicine Lake Highlands, CA              | 50.11            | 20.86                          | 9.10                           | 10.54 | 3.27  | 0.47              | 1.10             | 0.18             | 0.13                          | 4.06 |      | 99.82  |
| LGF700D                   | 3                   | Lower Ginkgo Fm., Col. River Basalt Grp. | 50.37            | 13.40                          | 14.80                          | 3.69  | 8.54  | 2.86              | 1.17             | 3.35             | 0.77                          | 0.21 | 0.85 | 100.01 |
| LGF700C                   | 3                   | Lower Ginkgo Fm., Col. River Basalt Grp. | 51.23            | 13.73                          | 14.29                          | 3.46  | 8.40  | 2.85              | 1.43             | 3.33             | 0.68                          | 0.20 | 0.40 | 100.00 |
| <i>Basaltic Andesites</i> |                     |  |                  |                                |                                |       |       |                   |                  |                  |                               |      |      |        |
| 83-35                     | 1                   | Callahan Flows, Medicine Lake, CA        | 54.20            | 17.60                          | 7.65                           | 5.88  | 8.82  | 3.66              | 0.95             | 0.95             | 0.17                          | 0.13 |      | 100.01 |
| <i>Andesites</i>          |                     |  |                  |                                |                                |       |       |                   |                  |                  |                               |      |      |        |
| 83-22                     | 1                   | Callahan Flows, Medicine Lake, CA        | 57.50            | 17.10                          | 6.75                           | 4.82  | 7.53  | 3.70              | 1.48             | 0.85             | 0.16                          | 0.12 |      | 100.01 |
| 79-39d                    | 1, 2                | Medicine Lake Highlands, CA              | 57.15            | 16.03                          | 7.53                           | 4.29  | 7.27  | 3.33              | 1.82             | 1.17             | 0.52                          | 0.11 |      | 99.22  |
| MVO-A                     | 3                   | Montserrat Volcano, Martinique           | 58.56            | 17.19                          | 7.39                           | 2.95  | 7.60  | 3.37              | 0.82             | 0.61             | 0.15                          | 0.18 | 0.12 | 98.94  |
| HK-1                      | 1, 2                | Hakone volcano, Japan                    | 59.52            | 16.79                          | 8.64                           | 2.14  | 6.20  | 3.21              | 0.86             | 1.01             | 0.15                          | 0.16 |      | 98.52  |
| HK-3                      | 1, 2                | Hakone volcano, Japan                    | 59.52            | 16.79                          | 8.64                           | 2.14  | 6.20  | 3.21              | 0.86             | 1.01             | 0.15                          | 0.16 |      | 98.52  |
| HK-5                      | 1, 2                | Hakone volcano, Japan                    | 59.52            | 16.79                          | 8.64                           | 2.14  | 6.20  | 3.21              | 0.86             | 1.01             | 0.15                          | 0.16 |      | 98.52  |
| <i>Dacites</i>            |                     |  |                  |                                |                                |       |       |                   |                  |                  |                               |      |      |        |
| BB-DR                     | 3                   | Black Butte, California                  | 65.68            | 17.23                          | 3.36                           | 1.93  | 5.07  | 4.44              | 1.18             | 0.41             | 0.11                          | 0.05 | 0.52 | 99.99  |
| 2524                      | 3                   | Dacite Porphyry, Helena, Montana         | 65.70            | 15.12                          | 2.94                           | 2.16  | 3.78  | 3.75              | 2.82             | 0.41             | 0.13                          | 0.05 | 3.38 | 100.25 |

<sup>a</sup>References are as follows: 1, *Kinzler et al.* [2000]; 2, *Wyatt et al.* [2001]; 3, this study.

samples (LGF700D, LGF700C, MVO-A, BB-DR, 2524a) were acquired by the first author; the remaining samples were provided by T. L. Grove (83-35 and 83-22, described by *Kinzler et al.* [2000]) or were selected from the more sodic modeled compositions (79-35i, 79-3b, 79-39d, HK-1, HK-3, and HK-5) of *Wyatt et al.* [2001]. Rocks were divided into three portions for various analyses. Thin sections of each rock specimen were used for petrographic and electron microprobe analyses (Figure 4). Six grams of each sample were ground into clay-sized particles for XRF analysis, and 3 cm diameter circular rock slabs were cut for spectral analysis.

### 2.1.2. Petrography and Modal Mineralogy

[10] All samples except 79-35i have porphyritic textures with variable amounts of euhedral to subhedral plagioclase, pyroxene, olivine, and amphibole phenocrysts. Dacites contain potassium feldspar, amphibole, and quartz phenocrysts. Plagioclase and pyroxene phenocrysts commonly display strong and weak zoning patterns, respectively. Most groundmass plagioclase was too fine-grained to determine its compositional heterogeneity. Mesostasis is commonly composed of smaller grains of the phenocryst minerals plus abundant glass and oxide phases. Magnetite, ilmenite, and minor (<2%) amounts of rutile are present. *Milam* [2002] provides detailed petrographic descriptions of rocks used in this study.

[11] Modal mineralogy for each rock was determined using a Cameca SX-50 electron microprobe at the University of Tennessee by Energy Dispersive Spectrometer (EDS) analyses using the Feature Scan technique [*Taylor et al.*, 1996]. EDS analyses were performed in 8–15  $\mu\text{m}$  steps (depending on the size of the sample area chosen) over grid areas representative of the entire sample. Classification of phases was dependent upon percent contributions of elements to the spectrum from each EDS analysis [*Milam*, 2002]. This procedure typically yielded  $\sim 150,000$  analyses per sample. Percentages of unclassified phases varied from 5–17 %, dependent upon grain size of mesostasis. Some of the finest groundmass had grains with dimensions of  $1 \times$

2  $\mu\text{m}$ , so that many grain boundaries were sampled, leading to a relatively higher percentage of unclassified phases. On the basis of observations of backscattered electron (BSE) images of mesostasis phases and EDS analyses, we assume that phases in the fine-grained unclassified mesostasis have similar relative abundances as the larger measured phases.

### 2.1.3. Geochemistry

[12] Bulk rock chemistries for rock samples were determined using X-ray fluorescence (XRF) (Table 1) by Act-Labs laboratories in Tuscon, Arizona, using procedures described by *Norrish and Hutton* [1969]. Normative mineralogies were calculated from XRF analyses. Anorthite contents from CIPW-NORM calculations are reported in Table 2.

[13] Chemical analyses by electron microprobe determined plagioclase compositions and the presence of zoning by use of core-to-rim transects equally spaced across individual plagioclase phenocrysts and groundmass. Analyses used an accelerating voltage of 15 kV, beam current of 20 nA, and counting times of 20 s per element. A 5 or 10  $\mu\text{m}$  size beam was used for coarsely zoned plagioclase phenocrysts, whereas 1, 2, or 5  $\mu\text{m}$  beams were used for plagioclase in mesostasis (typically <20  $\mu\text{m}$  diameter). ZAF (Z is atomic number, A is absorption, and F is fluorescence) corrections for matrix effects were applied to all analyses.

[14] Weighted average plagioclase compositions for each sample were calculated from microprobe analyses and point counting (Table 2) and used as a standard of comparison to modeled compositions (Table 2). Table 3 shows data and methods used to calculate weighted average plagioclase compositions. Point counting with an optical microscope (2000 cts/sample, 290  $\mu\text{m}$  step size) was used to measure modal abundances of total groundmass, plagioclase phenocrysts, and other phenocrysts for each sample (Table 3, columns 1–3, respectively). Feature Scan analyses were used to determine total plagioclase abundance for each rock (Table 3, column 4). The plagioclase groundmass abundance within the rock (column 6) was determined by taking the difference between total (column 4) and phenocryst

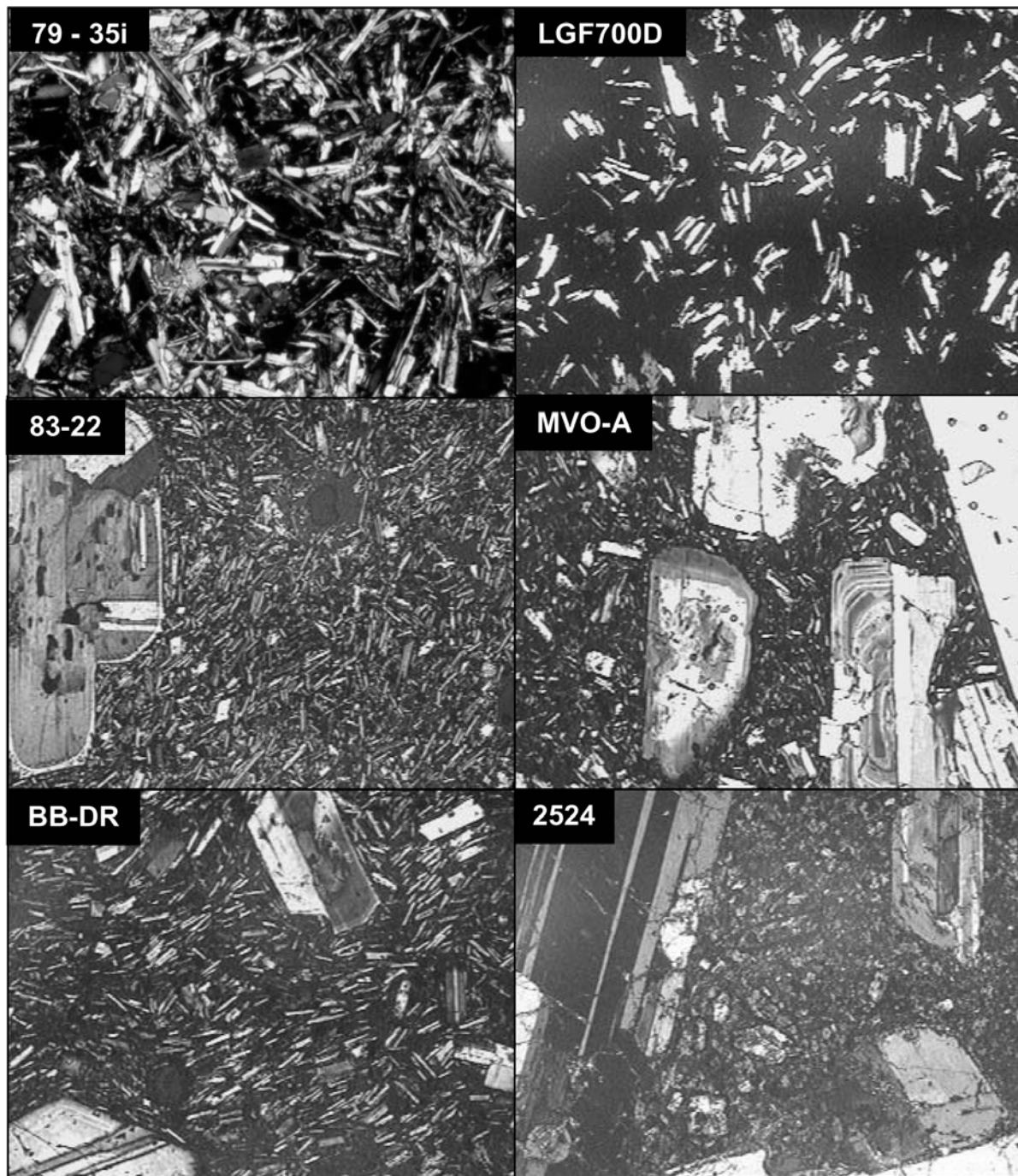


**Figure 4.** Photomicrographs of representative rock samples in part 1. Samples include basalts, basaltic andesites, and dacites. All samples but 79-35i are porphyritic with plagioclase phenocrysts. Note zoning in samples 83-22, MVO-A, BB-DR, and 2524. Widths of each photomicrograph are 1.8 mm.

plagioclase abundances (column 5). Plagioclase ground-mass and phenocryst abundances were then normalized to reveal the percentage of total plagioclase present as each grain type (columns 7 and 8). Plagioclase compositions for each grain type were calculated by averaging electron microprobe analyses for each grain type (columns 9 and 10). The lever rule was then used to calculate the weighted average plagioclase compositions (column 11) for each sample by inputting relative abundances (columns 7 and 8)

and averaged compositions for each of the grain types (columns 9 and 10).

#### 2.1.4. Spectral Analyses and Deconvolutions

[15] Polished rock slabs were used for spectral analysis. Polishing results in spectra with deeper absorption bands as compared to spectra of irregular, potentially weathered surfaces. Polished rock slabs used for spectral acquisition effectively present a coherent surface that acts like much larger grains. Samples were heated until a sample temper-

**Table 2.** Spectrally Modeled, NORM-Calculated, and Microprobe Weighted Average Ans for Plagioclase in Rocks of Part 1

| Sample  | Modeled An | NORM-Calculated An | Weighted Average An | RMS Error |
|---------|------------|--------------------|---------------------|-----------|
| 79-35i  | 74.2       | 64.6               | 74.2                | 0.005     |
| 79-3b   | 64.0       | 58.2               | 65.0                | 0.004     |
| LGF700D | 69.0       | 44.2               | 48.5                | 0.007     |
| LGF700C | 57.0       | 44.4               | 56.5                | 0.005     |
| 83-35   | 49.4       | 46.7               | 55.2                | 0.005     |
| 79-39d  | 69.2       | 44.0               | 59.2                | 0.006     |
| 83-22   | 56.8       | 43.6               | 60.3                | 0.004     |
| MVO-A   | 50.0       | 49.3               | 51.9                | 0.004     |
| HK-1    | 50.6       | 50.1               | 52.8                | 0.007     |
| HK-3    | 56.5       | 50.1               | 59.3                | 0.005     |
| HK-5    | 58.6       | 50.1               | 60.9                | 0.005     |
| BB-DR   | 32.7       | 37.2               | 49.3                | 0.005     |
| 2524a   | 18.3       | 32.3               | 13.8                | 0.005     |

ature of 80°C was reached and maintained throughout the experiment by a thermostatically controlled heating element. Spectra were collected using a Nicolet Nexus 670 spectrometer at Arizona State University. Each rock spectrum is the average of 180 scans and collected over the 2000–200 cm<sup>-1</sup> range (2.5–50 μm) with 2 cm<sup>-1</sup> spectral sampling. Sample radiance was then converted to emissivity and calibrated using techniques described by *Christensen and Harrison* [1993] and *Ruff et al.* [1997].

[16] The modal mineralogies of the rocks were modeled from their infrared emission spectra using a linear deconvolution algorithm [*Ramsey and Christensen*, 1998]. This algorithm is based on the assumption that a rock spectrum is a linear mixture of its constituent mineral spectra in proportion to the areal exposure of minerals. Deconvolutions of rock spectra for this part of the study were performed at laboratory spectral resolution (4 cm<sup>-1</sup>) using the end-member set from *Wyatt et al.* [2001] (Table 4). This end-member set includes eight homogeneous plagioclases ranging from An<sub>8</sub> to An<sub>92</sub> (Tables 4 and 5). Deconvolutions parameters similar to the *Wyatt et al.* [2001] were used to more closely compare with results from that study. Although emission spectra were collected over 2000–

200 cm<sup>-1</sup>, spectra were deconvolved over the 1280–400 cm<sup>-1</sup> range (as per *Wyatt et al.* [2001]). At higher wave numbers there are no fundamental silicate features above 1400 cm<sup>-1</sup> and although TES covers the wave number range of 1650–200 cm<sup>-1</sup>, at the time of the initial study, the laboratory spectrometer used did not measure the 400–200 cm<sup>-1</sup> region. Future work will make full use of the expanded range. Results from the deconvolution algorithm include a modeled spectrum, the percentages of spectral end-members used in the deconvolution, and a root-mean-square (RMS) error value [*Ramsey and Christensen*, 1998]. Spectral end-member percentages reflect mineral abundances in the rock for each mineral present [*Thomson and Salisbury*, 1993; *Hamilton et al.*, 1997; *Feely and Christensen*, 1999; *Hamilton and Christensen*, 2000; *Wyatt et al.*, 2001]. Visual comparison of measured and modeled spectra provided an initial indication of goodness of fit. RMS errors also indicate goodness of fit for a specific iteration of the model for a given sample.

## 2.2. Sand Mixtures: Plagioclase Zoning

### 2.2.1. Sample Acquisition

[17] Samples of large plagioclase crystals were collected from the Upper and Lower Ginkgo Flows of the Columbia River Basalt Group near the Willamette River in Portland, Oregon, the Steens River Basalts along the western flank of Steens Mountain, Harney County, Oregon, and the Sunstone Public Collecting Area in Lake County, Oregon. J. T. Gutmann (Wesleyan University) provided large plagioclase phenocrysts from the Pinacate Volcanic Field, Mexico. Phenocrysts were chosen because of their relative ease of extraction from bulk rock samples and the ability to collect large amounts of them. Other candidate samples were purchased from Ward's Scientific Supply Co.

### 2.2.2. Sample Selection

[18] Specimens were characterized using the optical microprobe and electron microprobe to determine the appropriateness (lack of compositional heterogeneity) of their use in this study. Samples showing signs of weathering/alteration or having relatively high percentages (≥5%)

**Table 3.** Data and Calculations for Weighted Average Plagioclase Compositions in Part 1

| Sample  | Percentage of Total Rock      |                                      |                                | Total Rock Calculations, %     |                                      |                        | Percent of Total Plagioclase |             | Plagioclase Compositions |                          | Sample Average An |
|---------|-------------------------------|--------------------------------------|--------------------------------|--------------------------------|--------------------------------------|------------------------|------------------------------|-------------|--------------------------|--------------------------|-------------------|
|         | Total Groundmass <sup>a</sup> | Plagioclase Phenocrysts <sup>a</sup> | Other Phenocrysts <sup>a</sup> | Total Plagioclase <sup>b</sup> | Plagioclase Phenocrysts <sup>a</sup> | Plagioclase Groundmass | Percent                      | Percent     | An of                    | An of                    |                   |
|         |                               |                                      |                                |                                |                                      |                        | Plagioclase                  | Plagioclase | Groundmass <sup>c</sup>  | Phenocrysts <sup>c</sup> |                   |
| 79-35i  | 100                           | 0                                    | 0                              | 100                            | 0                                    | 100                    | 100                          | 0           | 74.2                     | 0                        | 74.2              |
| 79-3b   | 92.4                          | 5.4                                  | 1.7                            | 46                             | 5.4                                  | 40.6                   | 88.3                         | 11.7        | 55.0                     | 80.1                     | 65.0              |
| LGF700D | 97.1                          | 2.35                                 | 0.55                           | 33.93                          | 2.35                                 | 31.58                  | 93.1                         | 6.9         | 47.8                     | 57.6                     | 48.5              |
| LGF700C | 95.68                         | 1.3                                  | 0                              | 49.12                          | 1.3                                  | 47.82                  | 97.0                         | 3.0         | 43.1                     | 56.8                     | 43.5              |
| 83-35   | 99.7                          | 0.3                                  | 0.05                           | 60.41                          | 0.3                                  | 60.11                  | 99.0                         | 1.0         | 55.3                     | 42.4                     | 55.2              |
| 79-39d  | 92.9                          | 5.4                                  | 1.7                            | 46                             | 5.4                                  | 40.6                   | 40.0                         | 60.0        | 59.6                     | 56.0                     | 59.2              |
| 83-22   | 93.65                         | 4.4                                  | 0.1                            | 51.16                          | 4.4                                  | 46.76                  | 91.4                         | 8.6         | 60.7                     | 56.1                     | 60.3              |
| MVO-A   | 61.7                          | 26.5                                 | 11.8                           | 49.32                          | 26.5                                 | 22.82                  | 46.3                         | 53.7        | 45.1                     | 57.6                     | 51.9              |
| HK-1    | 81.7                          | 14                                   | 4.3                            | 53                             | 14                                   | 39                     | 73.6                         | 26.4        | 47.0                     | 68.8                     | 52.8              |
| HK-3    | 59.75                         | 30.7                                 | 9.55                           | 56                             | 30.7                                 | 25.3                   | 45.2                         | 54.8        | 54.8                     | 63.0                     | 59.3              |
| HK-5    | 50                            | 31.95                                | 18.05                          | 53                             | 31.95                                | 21.05                  | 39.7                         | 60.3        | 39.7                     | 64.1                     | 60.9              |
| BB-DR   | 89.2                          | 7.5                                  | 3.2                            | 49.43                          | 7.5                                  | 41.93                  | 84.8                         | 15.2        | 47.0                     | 62.4                     | 49.3              |
| 2524a   | 58.5                          | 29.55                                | 12                             | 37.63                          | 29.55                                | 8.08                   | 21.5                         | 78.5        | 13.8                     | 30.5                     | 13.8              |

<sup>a</sup>Point counting.

<sup>b</sup>Feature scan analyses.

<sup>c</sup>Electron microprobe analyses.

**Table 4.** Bulk Chemistries of All Plagioclase End-Members Used in Study

| Sample                   | Mineral Name | Source | SiO <sub>2</sub> | Al <sub>2</sub> O <sub>3</sub> | FeO (Fe <sub>2</sub> O <sub>3</sub> ) | MnO  | MgO  | CaO  | Na <sub>2</sub> O | K <sub>2</sub> O | Total | An Number |
|--------------------------|--------------|--------|------------------|--------------------------------|---------------------------------------|------|------|------|-------------------|------------------|-------|-----------|
| WAR-0235                 | albite       | ASU    | 68.3             | 20                             | 0.33                                  | 0.01 | 0.04 | 0.01 | 11.5              | 0.02             | 100   | <1        |
| WAR-0244                 | albite       | ASU    | 69.2             | 18.2                           | 0.24                                  | 0.01 | 0.01 | 0.38 | 10.2              | 0.66             | 98.9  | 2         |
| WAR-0612                 | albite       | ASU    | 67.2             | 19                             | 0                                     | 0.02 | 0.4  | 0.35 | 9.26              | 0.18             | 96.4  | 2         |
| 5851 <sup>a</sup>        | albite       | UT     | 67.9             | 19.9                           | 0                                     | 0.02 | 0.02 | 0.63 | 9.71              | 0.27             | 98.5  | 2         |
| WAR-5851 <sup>b</sup>    | albite       | ASU    | 63               | 19.7                           | 5.51                                  | 0.02 | 0.47 | 1.37 | 8.5               | 0.22             | 98.8  | 8         |
| BUR-060D                 | oligoclase   | ASU    | 63.5             | 22.5                           | 0.21                                  | 0.01 | 0.01 | 3.36 | 9.21              | 0.6              | 99.4  | 15        |
| BUR-060                  | oligoclase   | ASU    | 60.4             | 21.9                           | 4.16                                  | 0.08 | 0.06 | 3.24 | 9.37              | 0.79             | 100   | 16        |
| WAR-5804 <sup>b</sup>    | oligoclase   | ASU    | 62               | 24                             | 0.04                                  | 0    | 0    | 4.74 | 9.03              | 0.5              | 100   | 22        |
| WAR-3680                 | oligoclase   | ASU    | 63.5             | 22.7                           | 0.03                                  | 0.13 | 0.44 | 4.94 | 7.76              | 0.63             | 100   | 25        |
| WAR-0234                 | oligoclase   | ASU    | 60.8             | 22.1                           | 0                                     | 0.02 | 0.85 | 5.37 | 6.71              | 0.91             | 96.8  | 29        |
| BUR-240 <sup>b</sup>     | andesine     | ASU    | 53.9             | 27.1                           | 0.53                                  | 0.01 | 0.07 | 9.51 | 5.55              | 0.34             | 97    | 48        |
| WAR-3080A                | andesine     | ASU    | 53.4             | 26.3                           | 1.5                                   | 0.03 | 0.65 | 9.62 | 4.94              | 1.2              | 97.6  | 48        |
| WAR-0024                 | andesine     | ASU    | 56.4             | 24.6                           | 0.06                                  | 0.07 | 2.51 | 9.38 | 4.67              | 0.76             | 98.5  | 50        |
| 4512A-L <sup>a</sup>     | labradorite  | UT     | 54.2             | 24.4                           | 2.16                                  | 0.05 | 1.32 | 9.8  | 4.34              | 1.3              | 97.6  | 51        |
| 0022 <sup>b</sup>        | labradorite  | UT     | 54.8             | 26.5                           | 1.1                                   | 0.03 | 0.24 | 10.4 | 4.02              | 0.47             | 97.6  | 53        |
| WAR-4524 <sup>b</sup>    | labradorite  | ASU    | 52.6             | 27.7                           | 2.5                                   | 0.02 | 0.14 | 10.9 | 5.01              | 0.42             | 99.3  | 53        |
| WAR-1384                 | labradorite  | ASU    | 51.3             | 30.9                           | 0.32                                  | 0.03 | 0.5  | 11.8 | 3.64              | 0.26             | 98.8  | 63        |
| WAR-RGAND01 <sup>b</sup> | labradorite  | ASU    | 49.9             | 28                             | 3.09                                  | 0.03 | 0.68 | 13   | 3.46              | 0.22             | 98.4  | 67        |
| SS <sup>a</sup>          | labradorite  | UT     | 50.9             | 29.8                           | 0.3                                   | 0.02 | 0.15 | 13.4 | 3.42              | 0.14             | 98.1  | 68        |
| WAR-5859 <sup>b</sup>    | bytownite    | ASU    | 48.4             | 31.5                           | 1.56                                  | 0.01 | 0.26 | 14.7 | 2.89              | 0.09             | 99.4  | 73        |
| 1382a <sup>a</sup>       | bytownite    | UT     | 49.1             | 30.4                           | 0.5                                   | 0.04 | 0.45 | 14.5 | 2.86              | 0.2              | 98.1  | 73        |
| WAR-5759 <sup>b</sup>    | bytownite    | ASU    | 41.5             | 29.5                           | 9.2                                   | 0.03 | 2.69 | 15.4 | 1.13              | 0.08             | 99.5  | 88        |
| BUR-340 <sup>b</sup>     | anorthite    | ASU    | 43.2             | 35.6                           | 0.54                                  | 0.01 | 0.39 | 17.6 | 0.84              | 0.01             | 98.2  | 92        |

<sup>a</sup>Samples added for this study.<sup>b</sup>Indicates end-members from [Wyatt *et al.*, 2001].

of impurities were excluded. Any plagioclase that displayed optical or compositional zoning was excluded. As one measure of compositional heterogeneity, fused bead analyses were performed. Portions of each plagioclase were ground into silt/clay-sized particles and placed on molybdenum strips. Each strip was placed between two electrodes and the current was slowly increased, thus increasing the temperature of the metal strip to above the plagioclase

liquidus. After complete melting, the electric current was then shut off to allow the plagioclase melt to be quenched into glass. Twenty-four electron microprobe analyses measured plagioclase compositions for each fused bead [Milam, 2002]. Plagioclases that demonstrated compositional variability >5 An were excluded from this study. Of the acquired samples, five (Table 4) were ultimately chosen that met the above selection criteria. Figure 5 shows the

**Table 5.** Plagioclase End-Member Sets Used in Deconvolutions From Part 2<sup>a</sup>

| End-Member Set | Set 1: Pure End-Members <sup>b</sup> | Set 2: 15 An Number Spacing | Set 3: Wyatt <i>et al.</i> [2001] | Set 4: All Plagioclase | Set 5: Plagioclase-Minus |
|----------------|--------------------------------------|-----------------------------|-----------------------------------|------------------------|--------------------------|
| A              | 5851                                 | WAR-0235                    | WAR-5851                          | WAR-0235               | WAR-0235                 |
| A              | 1382                                 | BUR-060D                    | WAR-5804                          | WAR-0244               | WAR-0244                 |
| A              |                                      | WAR-0234                    | BUR-240                           | WAR-0612               | WAR-0612                 |
| B              | 5851                                 | WAR-1384                    | WAR-4524                          | WAR-1384               | WAR-1384                 |
| B              |                                      | BUR-240                     | WAR-RGAND01                       | WAR-5851               | WAR-5851                 |
| B              |                                      | 1382                        | WAR-5859                          | BUR-060D               | BUR-060D                 |
| C              | 5851                                 | BUR-340                     | BUR-340                           | BUR-060                | BUR-060                  |
| C              | 4512                                 |                             | WAR-5759                          | WAR-5804               | WAR-5804                 |
| C              |                                      |                             |                                   | WAR-3680               | WAR-3680                 |
| D              | 5851                                 |                             |                                   | WAR-0234               | WAR-0234                 |
| D              | 0022                                 |                             |                                   | BUR-240                | BUR-240                  |
| D              |                                      |                             |                                   | WAR-3080A              | WAR-3080A                |
| E              | 1382                                 |                             |                                   | WAR-0024               | WAR-0024                 |
| E              | 0022                                 |                             |                                   | WAR-4524               | WAR-4524                 |
| E              |                                      |                             |                                   | WAR-RGAND01            | WAR-RGAND01              |
| F              | 1382                                 |                             |                                   | WAR-5759               | WAR-5759                 |
| F              | 4512                                 |                             |                                   | WAR-5859               | WAR-5859                 |
| F              |                                      |                             |                                   | BUR-340                | BUR-340                  |
| G              | 1382                                 |                             |                                   | 4512A-L                |                          |
| G              | SS                                   |                             |                                   | 5851                   |                          |
| G              |                                      |                             |                                   | 1382a                  |                          |
| G              |                                      |                             |                                   | SS                     |                          |
| G              |                                      |                             |                                   | 0022b                  |                          |

<sup>a</sup>Samples labeled WAR are from Ward's Scientific, and samples labeled BUR are from Burnham Scientific. Those without either designation are from this study.<sup>b</sup>End-member sets here are used for each column of the matrix in Figure 8. For example, end-member set A is used to deconvolve mixtures 11, 21, and 31.

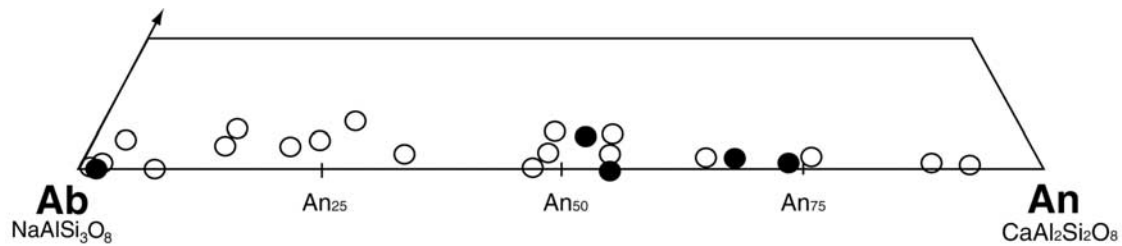


**Figure 5.** Analyzed compositions for spectral end-members from the ASU spectral library (open circles) and homogeneous plagioclases used in sand mixtures (solid circles).

compositional range ( $An_2$  to  $An_{73}$ ) of selected samples (solid circles).

### 2.2.3. Sample Preparation

[19] Selected plagioclase crystals were individually ground into particulate samples using mortar and pestle. These particulates were sieved and the coarse sand fraction (500–850  $\mu\text{m}$ ) was separated for use. Particles with visible impurities were extracted from each plagioclase sample. Samples were washed first by tap water and then twice with deionized water. Each particulate sample was then dried for 72 hours at 77°C. Each homogenous plagioclase sand was divided into two portions. Sand was poured (with no subsequent packing of grains) into 3 cm diameter sample cups. Thermal IR spectra of the samples were collected for use as spectral end-members in deconvolutions. The second portion was used in preparing compositional mixtures.

[20] The coarse sand size was chosen for several reasons. First, particle diameter must be larger than the wavelength of the emitted thermal infrared photons to avoid reduced spectral contrast [e.g., *Salisbury and Wald*, 1992; *Moersch and Christensen*, 1995; *Hamilton*, 1999]. The particle size range used in this study (500–850  $\mu\text{m}$ ) is well above the TIR wavelength range studied. Second, sand is the dominant particle size in most Martian dark regions that contributes to thermal emission spectra [*Christensen et al.*, 2001]. Finally, coarse sand particulates are oriented randomly during spectral measurements, eliminating potential grain orientation effects [*Ruff*, 1998].

### 2.2.4. Mixture Preparation

[21] In order to simulate zoning in plagioclase, homogeneous plagioclase samples were mixed in measured proportions (75–25%/50–50%/25–75%). A total of 21 mixtures that ranged in An variance ( $\Delta An = An$  (calcic plagioclase) –  $An$  (sodic plagioclase)) from  $\Delta An_{71}$  to  $\Delta An_9$  were produced (Figure 6).

### 2.2.5. Deconvolutions

[22] Deconvolutions of plagioclase mixture spectra were performed at laboratory (4  $\text{cm}^{-1}$ ), TES (10  $\text{cm}^{-1}$ ), Mini-TES (10  $\text{cm}^{-1}$ ), and THEMIS (10 bands from 6–15  $\mu\text{m}$  wavelength) spectral resolutions, the latter three simulating data that have been or will be collected of Mars. Figure 7 shows an example of measured spectra for a plagioclase mixture (11) at all 4 spectral resolutions. Deconvolutions of laboratory, TES, and Mini-TES resolution spectra include the wavelength range from 1300  $\text{cm}^{-1}$  to 400  $\text{cm}^{-1}$ . Use of this spectral range allows more direct comparisons of results to those of rock spectra deconvolutions (from part 1 of this study). Deconvolutions of spectra simulating TES data exclude a region (825–507  $\text{cm}^{-1}$ ,  $\sim 12$ –20  $\mu\text{m}$ ) affected

by atmospheric  $\text{CO}_2$  absorption on Mars. Although the spectral resolution of Mini-TES is equivalent to that of TES (in low-resolution mode), Mini-TES will conduct observations over a variety of atmospheric path lengths (from  $<2$  m to km). Atmospheric contributions to TIR spectra over such path lengths will be variable. At longer atmospheric path lengths, a broader wave number range (comparable to that of TES data) will be affected by atmospheric  $\text{CO}_2$ , with opacity increasing toward the center of the 667  $\text{cm}^{-1}$  (15- $\mu\text{m}$ )  $\text{CO}_2$  band. For near-field Mini-TES observations, however, the contribution of this  $\text{CO}_2$  absorption feature to the spectrum will be significantly reduced (M. D. Smith, personal communication, 2003). Such contributions will modify, but not obscure completely, features resulting from mineralogy. At the shortest path lengths ( $\sim 1$ –10 m) Mini-TES will observe, the contribution of  $\text{CO}_2$  to the spectrum is greatest ( $>1\%$ ) only between  $\sim 590$ –745  $\text{cm}^{-1}$  (M. D. Smith, personal communication, 2003), permitting a larger number of bands ( $\sim 25\%$  more on either side of the 667  $\text{cm}^{-1}$   $\text{CO}_2$  band) to be included in the deconvolution. To simulate short path length observations by Mini-TES, mixture spectra were deconvolved over this second, wider, spectral range. For deconvolutions at THEMIS resolution, band 10 was excluded because it is located in a region of atmospheric absorption. Bands 1 and 2 are identical and so represent only one wavelength range. Therefore end-member sets containing eight or less end-members were used in the THEMIS-simulated deconvolutions. Only spectral resolution and spectral range were considered in creating simulated TES, THEMIS, and Mini-TES data from our lab spectra. No attempt was made to consider the effects of other parameters such as signal-to-noise ratio (SNR) or atmospheric dust contributions.

[23] At laboratory, TES, THEMIS, and Mini-TES resolutions, each mixture spectrum was deconvolved using five different plagioclase end-member sets (Table 5) [*Milam*, 2002]: (1) a set containing only spectra from end-members used in physical mixtures, (2) a restricted set created by using spectral end-members spaced  $\sim 15$  An apart across the plagioclase solid-solution series, (3) another restricted set of end-members spanning the plagioclase solid-solution series from *Wyatt et al.* [2001], (4) a set containing all available plagioclase end-members from this study and the ASU spectral library [*Christensen et al.*, 2000], and (5) all available plagioclase end-members excluding those used in mixtures. The first end-member set was used as a “check” on the deconvolution technique, and was expected to model plagioclase compositions very precisely. Sets 2 and 3 were used to determine the suitability of using more

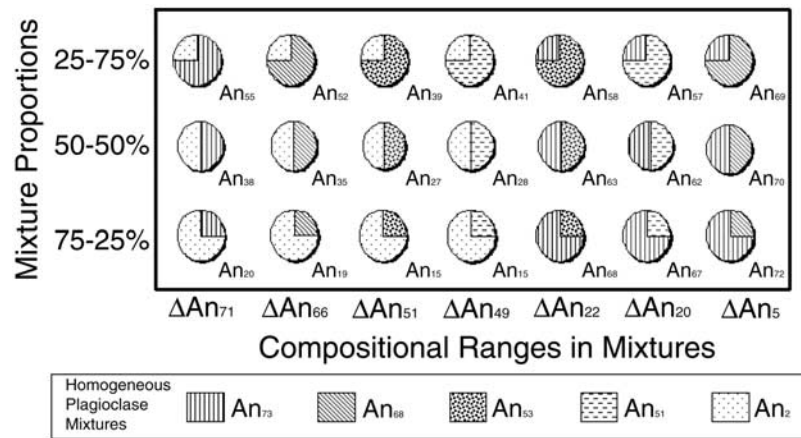


**Figure 6.** Matrix of two-component sand mixtures. Legend at bottom shows the compositions of homogeneous plagioclases used in the mixtures. Horizontal axis displays the variance of An between mixture components, whereas vertical axis displays mixture proportions. An number next to each pie chart refers to the average anorthite composition that results from each mixture.

restricted end-member sets in deconvolutions. The fourth end-member set represents a “best case” scenario, where some end-members are an exact match for those present in the sample. The fifth set is more representative of a remote-sensing scenario, because the likelihood of current spectral libraries containing end-members that are exact matches of plagioclase compositions on the Martian surface is relatively low. Deconvolution results were used to calculate plagioclase compositions (average An) for each mixture [Milam, 2002].

### 3. Results

#### 3.1. Rock Samples

[24] Measured and modeled spectra from rocks in this study are shown in Figure 8. Visual comparison of spectra shows that measured and modeled spectra correlate extremely well. RMS errors range from 0.004–0.005 for most samples, indicating reasonable spectral fits. Samples LGF700D and HK-1 have RMS errors of 0.007 and 79-39d has an RMS error of 0.006. Petrographic observations of LGF700D show some degree of weathering, with interstitial clays in the mesostasis. The spectral end-member set [Wyatt *et al.*, 2001] used here is not ideal for weathered igneous rocks due to its lack of spectra from weathering products, thus explaining the higher RMS error for this sample. Samples HK-1 and 79-39d do have fine-grained mesostasis with some interstitial glass. Because the [Wyatt *et al.*, 2001] end-member set contains only two glass spectral end-members, deconvolution may have resulted in higher RMS errors.

[25] Microprobe analyses of rock samples confirm that plagioclase phenocrysts are generally more calcic than groundmass plagioclase (Figure 9). Measured plagioclase compositional ranges typically become more sodic (lower An) and compositionally variable with increasing bulk-rock wt % SiO<sub>2</sub>. Compositional overlap among the grain types occurs, as expected from rocks that have undergone fractional crystallization. Phenocrysts show a variety of zoning patterns (normal, reverse, oscillatory) that vary among and within rock samples. Normal zoning is present but is not

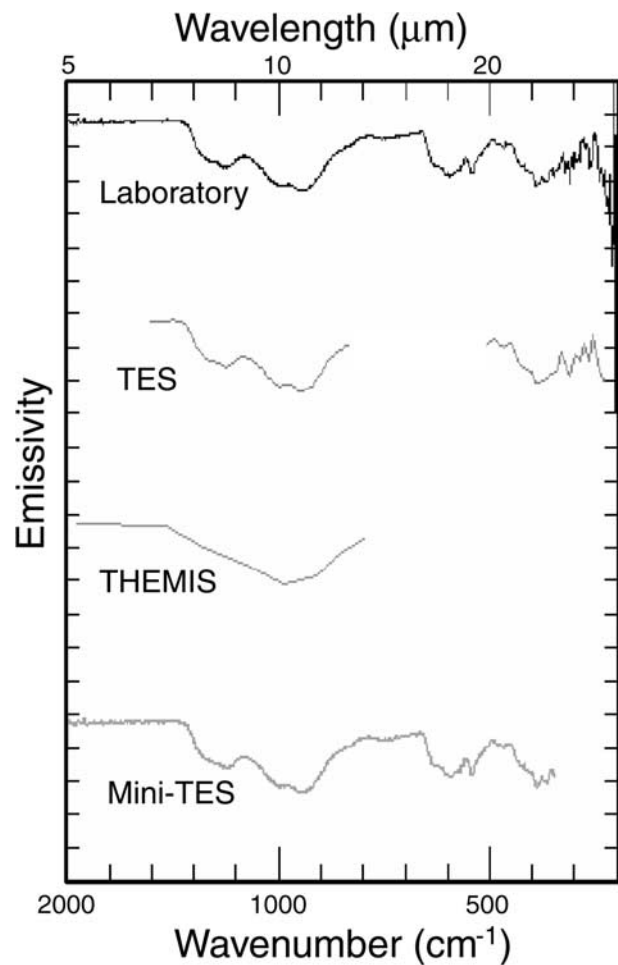


**Figure 7.** Spectra for plagioclase sand mixture 11 at laboratory, TES, THEMIS, and Mini-TES resolutions. Spectra are offset by 0.1 emissivity for clarity. Regions (825–507 cm<sup>-1</sup> and 1650–1300 cm<sup>-1</sup>) not used in deconvolutions of TES resolution spectra due to water vapor or CO<sub>2</sub> features were excluded.

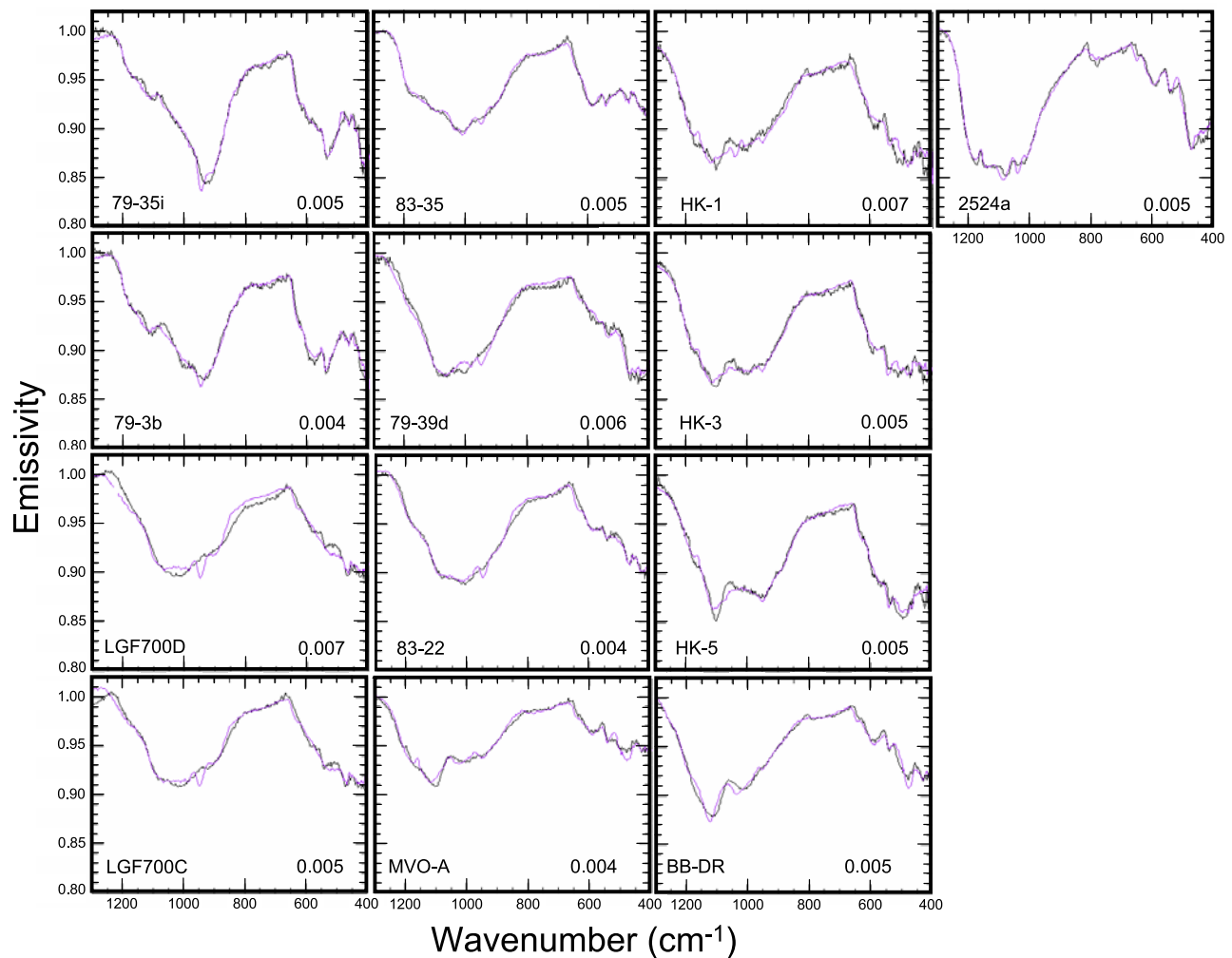


**Figure 8.** Measured (black) versus modeled (purple) spectra for volcanic rocks in part 1. Sample name is shown at the bottom left, and RMS error is shown on bottom right of each spectral plot. Horizontal axes represent wave number ( $\text{cm}^{-1}$ ), while vertical axes represent emissivity.

necessarily the dominant phenocryst zoning pattern in most rocks.

[26] Microprobe analyses of rocks with modeled plagioclase compositions outside measured compositional ranges in the *Wyatt et al.* [2001] study (HK-1, HK-3, HK-5) reveal that all modeled values actually lie within the remeasured compositional ranges (Figure 9). In the *Wyatt et al.* [2001] study, the tendency to analyze larger grains led to the appearance of more restricted plagioclase compositional ranges than are actually present. Because larger grains are typically more Ca-rich, these analyses excluded more of the sodic plagioclase. Average plagioclase compositions derived from the deconvolution results correlate well with the compositional range of the dominant grain type in each sample (Figure 9). In most samples plagioclase mesostasis has the highest areal (volume) percentage and so most modeled values are found to coincide with reported plagioclase mesostasis compositional ranges. In the few cases where plagioclase phenocrysts dominate (HK-3, HK-5, 2524a), modeled values fall mostly within measured plagioclase phenocryst compositional ranges (HK-3 and HK-5). The modeled composition for sample 2524a lies  $\sim 4$  An

outside of the phenocryst compositional range. This is likely due to the most sodic phenocrysts not being measured with microprobe analyses. Sample 79-3b contains sodic groundmass plagioclase and a separate, nonoverlapping assemblage of plagioclase phenocrysts (possibly xenocrysts), as illustrated in Figure 9. Although the spectrally modeled value for this sample falls within the measured compositional range for the dominant grain type (mesostasis in this case), this introduces the possibility of average compositions lying outside measured compositional ranges. Thus modeled values might represent an average plagioclase composition for a sample, but could potentially represent a composition not present in the rock.

[27] Although spectrally modeled values correlate with measured plagioclase compositional ranges, a more useful comparison of modeled and measured plagioclase can be made. Average plagioclase compositions for each rock were determined in two ways: as weighted averages of analyzed plagioclase compositions, and normative plagioclase compositions. Modeled compositions are typically within  $+10/-6$  An of weighted average values (Figure 9 and Table 2), and within the reported margins of error

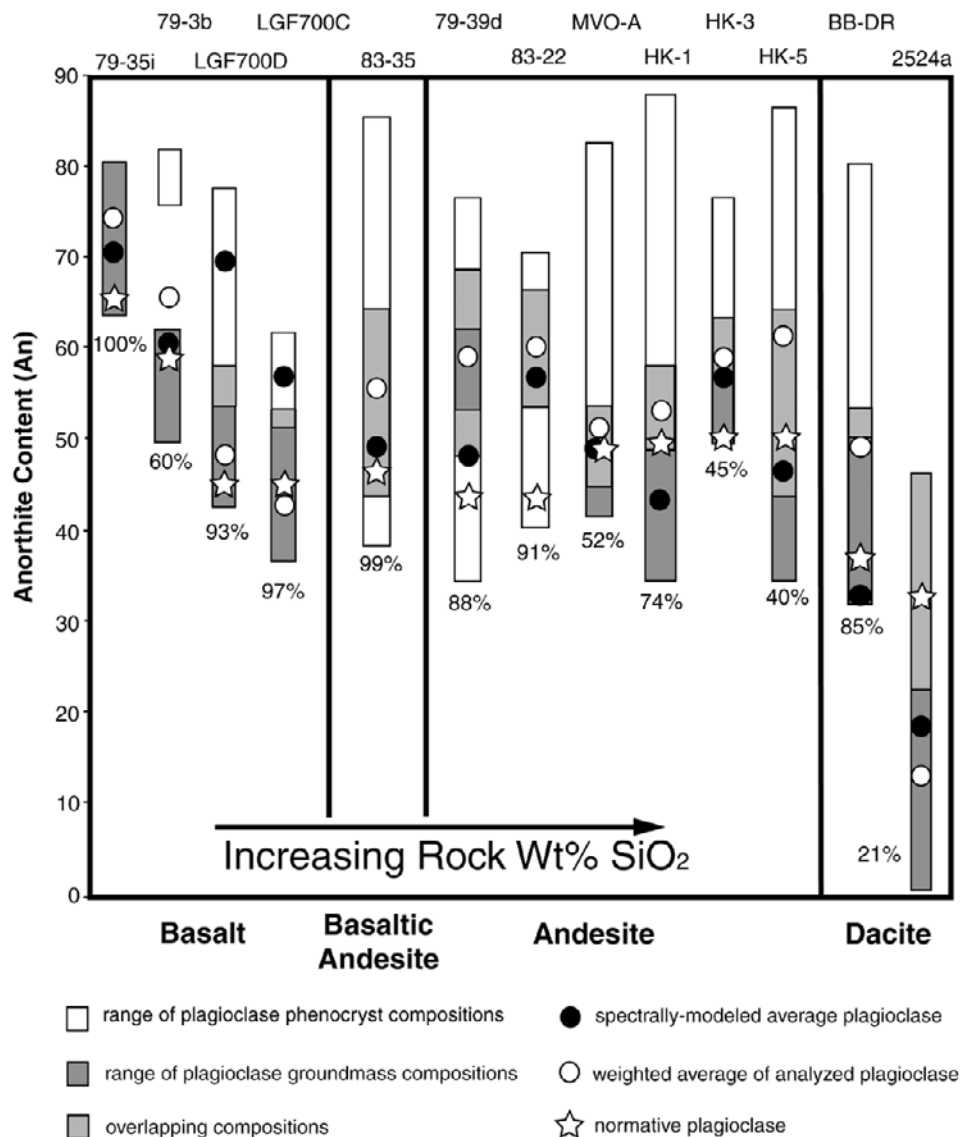


**Figure 9.** Comparison of spectrally modeled plagioclase compositions, weighted average of analyzed plagioclase compositions, calculated CIPW normative plagioclase compositions, and analyzed compositional ranges for each rock sample. Percentages indicate the proportion of total plagioclase that is groundmass. Sample numbers are shown at the top.

(10–15 An) of the technique [Hamilton *et al.*, 1997; Hamilton and Christensen, 2000; Hamilton *et al.*, 2001]. Samples LGF700D and BB-DR (+20/–17 An) are exceptions. When compared with normative plagioclase compositions for each sample (Figure 9 and Table 2), modeled values are typically within +13/–14 An, also within the reported margins of error (with the exception of samples LGF700D and BB-DR (+25/–5 An)).

### 3.2. Plagioclase Mixture Deconvolutions

[28] Analyses of the two-component physical mixture spectra at laboratory, TES, THEMIS, and Mini-TES spectral resolutions show that measured versus modeled spectra are well correlated. Figure 10 illustrates a representative example of measured versus modeled spectra at various resolutions. RMS errors for all deconvolutions ranged from 0.001–0.005. Deconvolved plagioclase compositions

at laboratory resolution ( $4\text{ cm}^{-1}$ ) can be modeled to within +8/–11 An and to within +9/–12 An of measured values at TES resolution ( $10\text{ cm}^{-1}$ ) for all end-member sets (Table 6). Modeled plagioclase compositions at THEMIS resolution are within +11/–12 An of measured values. At Mini-TES spectral resolution, modeled compositions are within +8/–12 An of measured values. Deconvolutions using the various end-member sets model both calcic and sodic plagioclase in sub equal amounts.

[29] So far, errors between spectrally modeled and analyzed plagioclase compositions have been reported as  $\pm$  An (Table 6). Errors reported in this way represent maximum error ranges, because they give equal weight to the most poorly modeled values. Standard deviations are more representative of the majority of compositions. Although plagioclase compositions can be modeled to within +8/11 An, +9/–12 An, +11/–12 An, and +8/–12

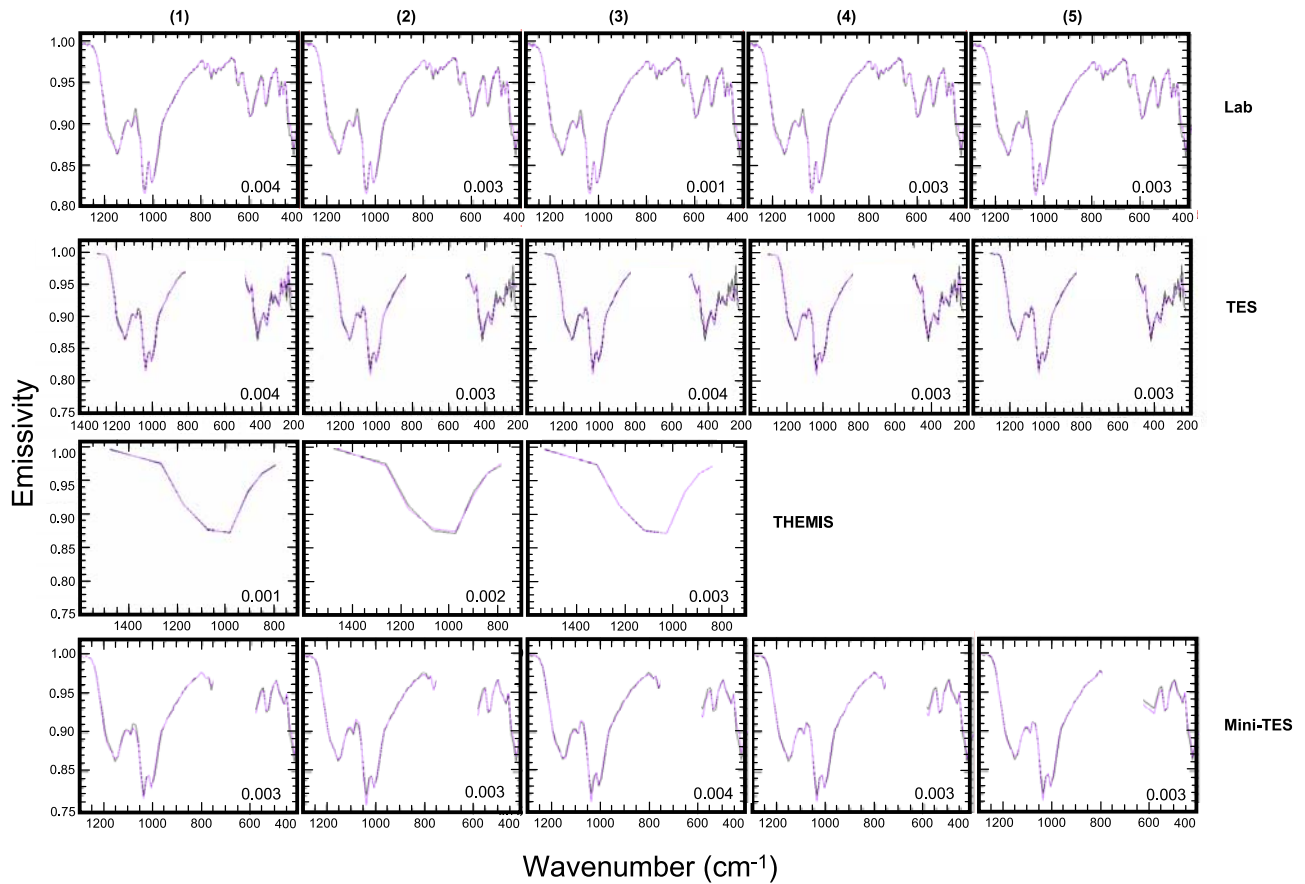


**Figure 10.** Measured (black) versus modeled (purple) spectra for  $An^{28}$  sand mixture in part 2 (Figure 6). RMS error for each deconvolution is shown in the bottom right corner of each spectral plot. Rows, from top to bottom, are at laboratory, TES, THEMIS, and Mini-TES resolutions, respectively. Columns, from left to right, utilize spectral end-member sets 1–5, respectively. Horizontal axis for each plot represents wave number ( $cm^{-1}$ ), while vertical axes represent emissivity.

An of measured values at laboratory, TES, THEMIS, and Mini-TES resolutions, the majority of modeled compositions were within  $\pm 4$  An ( $1\sigma$  standard deviation) at laboratory, TES, and Mini-TES resolutions and within  $\pm 6$  An at THEMIS resolution (Table 6).

## 4. Discussion

### 4.1. Rocks: Phenocrysts Versus Groundmass

#### 4.1.1. Origin of the Sodid Bias

[30] Plagioclase phenocrysts and groundmass in the terrestrial volcanic rocks studied here (and by *Wyatt et al.* [2001]) display a variety of zoning patterns (normal, oscillatory, reverse). Normal zoning cannot be assumed to be typical and the suggestion that more sodic-modeled plagioclase compositions are the result of the volumetric dominance of sodic rims on plagioclase phenocrysts [*Wyatt et al.*, 2001] is incorrect. Furthermore, an incomplete assessment of the plagioclase compositions [*Wyatt et al.*, 2001] gave the appearance that the linear deconvolution technique was not accurately modeling plagioclase compositions. Our new microprobe measurements more accurately represent the full range of plagioclase compositions for the rock samples in the *Wyatt et al.* [2001] study, showing that modeled compositions correspond to measured compositional ranges.

**Table 6.** Overall Results From Deconvolutions in Part 2 of This Study<sup>a</sup>

| Resolution | Embr | +An | −An | SD   | RMS    |
|------------|------|-----|-----|------|--------|
| Laboratory | 1    | 8   | −3  | 3.53 | <0.003 |
| Laboratory | 2    | 6   | −11 | 4.16 | <0.005 |
| Laboratory | 3    | 5   | −9  | 3.60 | <0.005 |
| Laboratory | 4    | 6   | −6  | 3.56 | <0.003 |
| Laboratory | 5    | 4   | −9  | 3.28 | <0.003 |
| TES        | 1    | 8   | −6  | 3.80 | <0.004 |
| TES        | 2    | 4   | −12 | 4.00 | <0.005 |
| TES        | 3    | 5   | −9  | 3.78 | <0.004 |
| TES        | 4    | 9   | −7  | 3.90 | <0.003 |
| TES        | 5    | 6   | −8  | 3.57 | <0.004 |
| THEMIS     | 1    | 11  | −3  | 3.80 | <0.002 |
| THEMIS     | 2    | 11  | −9  | 6.20 | <0.002 |
| THEMIS     | 3    | 4   | −12 | 3.92 | <0.005 |
| Mini-TES   | 1    | 8   | −4  | 3.33 | <0.004 |
| Mini-TES   | 2    | 4   | −12 | 3.92 | <0.005 |
| Mini-TES   | 3    | 6   | −9  | 3.89 | <0.005 |
| Mini-TES   | 4    | 6   | −7  | 3.71 | <0.003 |
| Mini-TES   | 5    | 6   | −9  | 3.54 | <0.003 |

<sup>a</sup>Results are grouped by resolution and end-member set used and are reported as variance ( $\pm An$ ) and  $1\sigma$  standard deviation. Maximum RMS errors for each set of deconvolutions are also shown.

[31] Our results suggest that the apparent sodic bias in modeled plagioclase compositions arises from the contribution of the areally (volumetrically) more abundant grain type in each sample. In most cases, a more sodic plagioclase groundmass dominates, shifting the modeled An to more sodic ends of the compositional range. Modeled plagioclase compositions correspond to the dominant grain type, reaffirming that linear mixing of the spectra of plagioclase phenocrysts and groundmass occurs. Most samples from this study (and probably most volcanic rocks) are dominated by groundmass plagioclase, which will produce modeled plagioclase compositions that are more sodic than median compositions, but accurately reflect the volumetrically dominant composition.

#### 4.1.2. Standards of Comparison

[32] When spectrally modeled average plagioclase compositions are compared to weighted averages of analyzed grains or normative plagioclase compositions, most results are broadly consistent with previous studies [Hamilton *et al.*, 1997; Hamilton and Christensen, 2000; Hamilton *et al.*, 2001], but small differences remain. Weighted averages of analyses and normative compositions for most rocks are not identical and it is unclear which of these standards provides the best estimate of average plagioclase composition.

##### 4.1.2.1. Weighted Average Compositions

[33] Weighted compositions were derived from microprobe analyses in which core-to-rim transects (in approximately equal intervals) were made across representative plagioclase phenocryst and groundmass grains. The number of analyses ranged from 8–15 for phenocrysts and 2–5 for groundmass grains. Analyses were averaged for each grain type (phenocryst and groundmass) separately. This method assumed that traverse analyses were representative of areal exposures of zones in plagioclase.

[34] This assumption has some level of uncertainty, however. Let us compare the average (from method mentioned above) and actual plagioclase compositions of a hypothetical plagioclase grain. The spherical grain (190  $\mu\text{m}$  total diameter) is normally zoned with 10 zones, each 10  $\mu\text{m}$  in width. Plagioclase compositions change 2 An from zone to zone and range from An<sub>75</sub>–An<sub>57</sub> in composition (a typical range for plagioclase in terrestrial basalts and andesites). For this example, we assume that 10 microprobe analyses were made in a core-to-rim transect through the center of the grain, with each analysis corresponding to the center of an individual zone. The average plagioclase composition (An<sub>66</sub>) for the phenocryst was derived by averaging all 10 microprobe analyses (the same manner in which phenocryst and groundmass averages were derived for this study, Table 3, columns 9 and 10). Thus each analysis is considered equally and not according to areal exposures in thin section. Factoring in areal exposures for each zone, the actual average composition of An<sub>63</sub> was determined. The same grain, but reversely zoned, yields an actual composition of An<sub>69</sub>. For this example, the average of microprobe analyses is within  $\pm 3$  An of the actual plagioclase composition. Similar comparisons of averaged and actual plagioclase compositions were made for other normal, reverse, and oscillatory zoned hypothetical grains (with variable compositional ranges, zone widths, and numbers of zones). Results indicate that average plagioclase

compositions derived from microprobe analyses are accurate within  $\pm 4$  An.

##### 4.1.2.2. Normative Compositions

[35] Calculated CIPW-Norms have long provided a means of comparing differences between volcanic rocks (usually those containing small-grained mesostasis whose modes cannot be measured by point-counting). Norm calculations utilize bulk chemical analyses to derive an idealized set of synthetic minerals for purposes of comparison. In natural samples, the normative phases may actually be absent from the rock or modeled in anomalous abundances. Imprecise modeling of calcium-rich phases, such as sphene or apatite, has the potential effect of affecting albite and anorthite abundances, which, in turn, affects the norm-derived average plagioclase composition for a rock. Variations between measured and normative mineral abundances do occur in rocks used in this study [Milam, 2002]. The CIPW-Norm calculation also assumes crystallization of mineral phases in equilibrium under dry conditions. The assumption of equilibrium, as applied to rocks used in this study, is problematic, as zoned plagioclase suggests disequilibrium conditions during fractional crystallization. All terrestrial volcanic rocks, especially those of intermediate compositions (andesite and dacite), experience crystallization under “wet” (<10 wt% H<sub>2</sub>O) conditions. Thus normative plagioclase compositions are modeled with an assumed set of conditions that are likely not present in most volcanic rocks.

## 4.2. Sand Mixtures: Plagioclase Zoning

[36] Results from the mixing study indicate that spectra from physical mixtures of homogenous plagioclase components produce a composite spectrum that is representative of the average plagioclase composition. Deconvolutions of plagioclase mixture spectra at laboratory, TES, THEMIS, and Mini-TES spectral resolutions produce modeled compositions that approximate average plagioclase compositions closer than previously reported [Hamilton *et al.*, 1997; Hamilton and Christensen, 2000; Hamilton *et al.*, 2001]. The only significant systematic errors can be correlated to changes in end-member sets. Results indicate that accuracy can be improved further by choice of the plagioclase end-member set input into the deconvolution algorithm. End-member sets were evaluated for their overall ability to determine average plagioclase compositions at all resolutions by comparison of An variance among different end-member sets and standard deviations from deconvolutions. Table 6 summarizes the results of these comparisons. Excluding the pure end-member sets that serve as a “check” to deconvolutions, the evaluation reveals that plagioclase compositions are better modeled by use of end-member sets (4 and 5) with a higher number of spectral end-members (i.e., all available plagioclase or all available plagioclase minus those used in the mixtures). More restricted end-member sets (2 and 3) typically produce larger ranges in An variance. This suggests that better modeled spectral fits result from use of expanded end-member sets and are more useful in determining plagioclase compositions. These results are consistent with previous studies [Feely and Christensen, 1999; Hamilton and Christensen, 2000].

[37] The linear deconvolution algorithm [Ramsey and Christensen, 1998] models measured spectra using a linear least squares fit and lacks the ability to distinguish between

a zoned plagioclase grain of a given composition and a physical mixture of plagioclase resulting in the same composition. Although the compositions of many spectral end-members used in the best fits correspond closely to the compositions present within each mixture, others do not. While accuracy in determining plagioclase compositions is improved with the addition of more spectral end-members (sets 4 and 5), significant amounts (>10%) of compositionally different (from those actually present) end-members are still chosen by the algorithm. Perhaps the addition of spectral end-members at smaller compositional intervals over the entire plagioclase solid solution series might permit the identification of distinct clusters of end-members that correspond to compositions in a rock.

## 5. Applications to Martian Remote Sensing

[38] Results from this study demonstrate the potential to which TES, THEMIS, and Mini-TES spectra may be deconvolved to derive plagioclase compositions. However, this study does not take into account atmospheric effects, effects from the addition of other mineral phases, or decreased signal-to-noise ratios. Such additions to TIR spectra likely reduce the degree to which compositions can be determined. As shown in this study, for example, the fidelity with which plagioclase compositions can be accurately derived is reduced between physical mixtures of feldspars (one phase in solid solution) versus rock samples (multiple mineral phases). However, knowing the approximate accuracy with which we can derive plagioclase compositions suggests a number of potential applications of this research. The ability to determine plagioclase compositions has the potential for the discrimination of individual volcanic units/lava flows, identification of source regions for landing site samples, comparison of global and regional Martian plagioclase compositions to Martian meteorites, and the identification of areas of subaqueous or hydrothermal alteration.

[39] In terrestrial volcanic centers, magmatic compositions often vary, reflecting changes in the degree of source region melting, fractional crystallization, assimilation, etc. Such evolution is expressed in the compositional variability of lava flows. Analysis of TES, THEMIS, and Mini-TES thermal emission spectra could potentially be used to identify compositionally distinct flow/rock units on the Martian surface in part by their plagioclase compositions. Using TES and Mini-TES data to determine anorthite contents and THEMIS data to produce maps of such units may provide a means of tracking the evolution of Martian magmas. Differences in plagioclase compositions greater than 10–15 An are likely to represent true compositional and/or mineralogical differences and would be suitable for such mapping. Deconvolved plagioclase compositions also can be used to measure compositional variability of laterally extensive lava flows on Mars. Terrestrial flow compositions can vary not only by eruptive episode, but also by proximity to the eruptive center. Plagioclase compositions can also provide information on crystallization temperature and have potential utility as geobarometers [Coskren and Blackburn, 1972; Nash, 1973].

[40] The detection of sodic plagioclase in basalts and andesites (which typically contain calcic plagioclase) has the potential for identifying regions on Mars where alter-

**Table 7.** Deconvolved Plagioclase Compositions From Surface Type I and II Spectra

| End-Member Set                  | Surface Type 1   | Surface Type II  |
|---------------------------------|------------------|------------------|
| <i>Bandfield et al.</i> [2000]  | An <sub>55</sub> | An <sub>63</sub> |
| <i>Wyatt et al.</i> [2001]      | An <sub>61</sub> | An <sub>59</sub> |
| <i>Wyatt and McSween</i> [2002] | An <sub>66</sub> | An <sub>60</sub> |
| 2 from this study               | An <sub>47</sub> | An <sub>34</sub> |
| 4 from this study               | An <sub>42</sub> | An <sub>34</sub> |

ation by aqueous or hydrothermal processes has occurred. On Earth, exposure of basalts to seawater results in the conversion of calcic plagioclase to albite [e.g., *Hardie*, 1983; *Alt and Emmermann*, 1985; *Stakes and Schiffman*, 1999]. Similar alteration occurs in hydrothermal systems [Whyte, 1966]. If Martian igneous rocks are shown to contain plagioclase with compositions <An<sub>30</sub>, those basalts/andesites may have experienced aqueous alteration, especially if other hydrothermal minerals are also present. Detection of albitic basalts could be used in a first order search for hydrothermal areas on Mars.

[41] Another application involves data sets from both orbiters and landers. Mini-TES will presumably collect spectra from individual rocks derived from a variety of geologic units. With Mini-TES's potential for discriminating plagioclase compositions, these data may be compared to plagioclase compositions of dust-free areas detected by TES and THEMIS across broader regions (3 × 6 km/pixel and 100 m/pixel) near the landing site. Thus source regions for individual rocks observed at landing sites might be identified, allowing geologic interpretation of an area beyond the short (<1 km) traverses of the MER rovers.

[42] Deconvolutions of surface type 1 and surface type 2 spectra [Bandfield et al., 2000] from Mars also provide insight into variability of Martian surface rocks. In Table 7, plagioclase compositions calculated from Bandfield et al. [2000] show surface type 1 is more sodic (An<sub>55</sub>) than surface type 2 (An<sub>63</sub>). More recent studies show opposite trends. Deconvolutions of TES spectra using end-member sets from Wyatt et al. [2001], Wyatt and McSween [2002], and sets 2 and 4 from this study (added to other nonplagioclase spectral end-members from Wyatt et al. [2001]) give varying plagioclase compositions among both surface types. Table 7 shows that modeled plagioclase compositions for surface type 1 range from An<sub>66</sub>–An<sub>42</sub> and An<sub>60</sub>–An<sub>34</sub> for surface type 2. These results are more consistent with the trend in terrestrial samples (Figures 2 and 9), with basalt typically containing more calcic plagioclase than andesite. Figure 11 shows that when compared to terrestrial and lunar basalts, modeled plagioclase compositions for Martian surface types are relatively sodic, consistent with Martian meteorites and studies showing enrichments in bulk-planet alkalis [Wänke and Dreibus, 1988] and Na and K in plagioclase [Papike, 1998]. If we assume that the end-member set containing the most plagioclase end-members (set 5; Table 7) produces more accurately modeled plagioclase compositions (as proposed earlier), then Martian plagioclase is even more sodic than the entire range suggests (Figure 11).

## 6. Summary

[43] Geochemical and spectral analyses of plagioclase-bearing rocks and plagioclase sand mixtures provide new

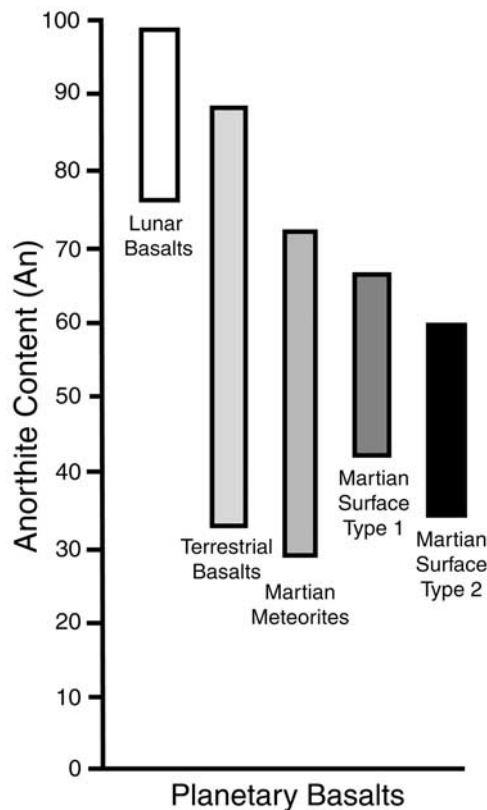


**Figure 11.** Summary of measured and derived plagioclase compositional ranges in lunar, terrestrial, and Martian basalts/surface types. Representative data for Martian meteorites are given by *McSween and Treiman* [1998].

insight into Martian remote-sensing capabilities and the potential for further investigations. Results from this study indicate that (1) plagioclase zoning patterns are highly variable and thus do not exert an overriding influence on spectrally modeled average plagioclase compositions; (2) measured plagioclase compositional ranges from the *Wyatt et al.* [2001] study did not encompass the complete compositional range present within rock samples, so that several deconvolved plagioclase compositions did not correlate with measured ranges; (3) sodic groundmass plagioclase is the volumetrically dominant grain type in most terrestrial volcanic rocks and thus its strong influence in thermal infrared spectra is appropriate; (4) modeled plagioclase compositions from volcanic rock spectra generally fall within  $+10/-6$  and  $+13/-14$  An of the weighted average of analyzed plagioclase and calculated normative plagioclase compositions, respectively; (5) compositional zones in plagioclase add linearly to produce composite spectra representative of average plagioclase compositions; (6) spectral deconvolutions of spectra of sand mixtures at laboratory, TES, THEMIS, and Mini-TES resolutions give plagioclase compositions to within  $+8/-11$  An,  $+9/-12$  An,  $+11/-12$  An, and  $+8/-12$  An of measured values ( $\pm 4$  An ( $1\sigma$  standard deviation) at laboratory, TES, and Mini-TES resolutions and  $\pm 6$  An at THEMIS resolution); and (7) in rocks and sand mixtures involving complex mixtures of plagioclase grains of varying compositions, average plagioclase compositions can be accurately derived. This study

supports the potential application of thermal emission spectroscopy in evaluating a variety of Martian geologic processes.

[44] **Acknowledgments.** This work was supported by the NASA Mars Data Analysis Program (NAG5-10525) to HYM and a student research grant from the Mayo Educational Foundation to KAM. We would like to thank Jeff Johnson (USGS), Josh Bandfield (ASU), and Larry Taylor (UT) for insightful reviews and comments of this work. Additional thanks to Allan Patchen (UT) for his assistance with use of the electron microprobe at the University of Tennessee.

## References

- Alt, J. C., and R. Emmermann (1985), Geochemistry of hydrothermally altered basalts: Deep Sea Drilling Project Hole 504B, Leg 83, *Initial Rep. Deep Sea Drill. Proj.*, 83, 249–262.
- Bandfield, J. L., V. E. Hamilton, and P. R. Christensen (2000), A global view of Martian surface compositions from MGS-TES, *Science*, 287, 1626–1630.
- Christensen, P. R., and S. T. Harrison (1993), Thermal infrared emission spectroscopy of natural surfaces: Application to desert varnish coatings on rocks, *J. Geophys. Res.*, 98, 19,819–19,834.
- Christensen, P. R., et al. (1992), Thermal Emission Spectrometer experiment: Mars Observer mission, *J. Geophys. Res.*, 97, 7719–7734.
- Christensen, P. R., J. L. Bandfield, V. E. Hamilton, D. A. Howard, M. D. Lane, J. L. Piatek, S. W. Ruff, and W. L. Stefanov (2000), A thermal emission spectral library of rock-forming minerals, *J. Geophys. Res.*, 105, 9735–9739.
- Christensen, P. R., et al. (2001), Mars Global Surveyor Thermal Emission Spectrometer experiment: Investigation description and surface science results, *J. Geophys. Res.*, 106, 23,823–23,871.
- Christensen, P. R., et al. (2003), Miniature Thermal Emission Spectrometer for the Mars Exploration Rovers, *J. Geophys. Res.*, 108(E12), 8064, doi:10.1029/2003JE002117.
- Christensen, P. R., et al. (2004), The Thermal Emission Imaging System (THEMIS) for the Mars 2001 Odyssey Mission, *Space Sci. Rev.*, in press.
- Coskren, D., and W. H. Blackburn (1972), Equilibration between aluminous pyroxene and plagioclase; A geobarometer-geothermometer, *Eos Trans. AGU*, 53, 549.
- Feely, K. C., and P. R. Christensen (1999), Quantitative compositional analysis using thermal emission spectroscopy: Application to igneous and metamorphic rocks, *J. Geophys. Res.*, 104, 24,195–24,210.
- Hamilton, V. E. (1999), The effect of particle size on rock spectra in the thermal infrared: Implications for TES data analysis, *Lunar Planet. Sci. [CD-ROM]*, XXX, Abstract 2001.
- Hamilton, V. E., and P. R. Christensen (2000), Determining the modal mineralogy of mafic and ultramafic igneous rocks using thermal emission spectroscopy, *J. Geophys. Res.*, 105, 9717–9733.
- Hamilton, V. E., P. R. Christensen, and H. Y. McSween Jr. (1997), Determination of Martian meteorite lithologies and mineralogies using vibrational spectroscopy, *J. Geophys. Res.*, 102, 25,593–25,603.
- Hamilton, V. E., M. B. Wyatt, H. Y. McSween Jr., and P. R. Christensen (2001), Analysis of terrestrial and Martian volcanic compositions using thermal emission spectroscopy: 2. Application to Martian surface spectra from the Mars Global Surveyor Thermal Emission Spectrometer, *J. Geophys. Res.*, 106, 14,733–14,746.
- Hardie, L. A. (1983), Origin of  $\text{CaCl}_2$  brines by basalt-seawater interaction: Insights provided by some simple mass balance calculations, *Contrib. Mineral. Petrol.*, 82(2–3), 205–213.
- Iiishi, K., T. Tomisaka, T. Kato, and Y. Umegaki (1971), Isomorphous substitution and infrared and far infrared spectra of the feldspar group, *Neues Jahrb. Mineral.*, 115, 98–119.
- Kinzler, R. J., J. M. Donnelly-Nolan, and T. L. Grove (2000), Late Holocene hydrous mafic magmatism at the Paint Pot Crater and Callahan flows, Medicine Lake Volcano, N. California and the influence of  $\text{H}_2\text{O}$  in the generation of silicic magmas, *Contrib. Mineral. Petrol.*, 138, 1–16.
- McSween, H. Y., Jr., and A. H. Treiman (1998), Martian meteorites, in *Planetary Materials*, edited by J. J. Papike, *Rev. Mineral.*, 36, 6-01–6-53.
- Milam, K. A. (2002), Accuracy of plagioclase compositions from laboratory and Mars spacecraft thermal emission spectra, M.S. thesis, Univ. of Tenn. at Knoxville, Knoxville.
- Moersch, J. E., and P. R. Christensen (1995), Thermal emission from particulate surfaces: A comparison of scattering models with measured spectra, *J. Geophys. Res.*, 100, 7465–7477.
- Nash, D. B., and J. W. Salisbury (1991), Infrared reflectance spectra (2.2–15  $\mu\text{m}$ ) of plagioclase feldspars, *Geophys. Res. Lett.*, 18, 1151–1154.
- Nash, W. P. (1973), Plagioclase resorption phenomena and geobarometry in basic lavas, *Eos Trans. AGU*, 57, 507.

- Norrish, K., and J. T. Hutton (1969), An accurate X-ray spectrographic method for the analysis of a wide range of geological samples, *Geochim. Cosmochim. Acta*, **33**, 431–453.
- Papike, J. J. (1998), Comparative planetary mineralogy: Chemistry of melt-derived pyroxene, feldspar, and olivine, in *Planetary Materials*, edited by J. J. Papike, *Rev. Mineral.*, **36**, 7-01–7-11.
- Ramsey, M. S., and P. R. Christensen (1998), Mineral abundance determination: Quantitative deconvolution of thermal emission spectra, *J. Geophys. Res.*, **103**, 579–596.
- Ruff, S. W. (1998), Quantitative thermal infrared emission spectroscopy applied to granitoid petrology, Ph.D. dissertation, 234 pp., Ariz. State Univ., Tucson.
- Ruff, S. W., P. R. Christensen, P. W. Barbera, and D. L. Anderson (1997), Quantitative thermal emission spectroscopy of minerals: A laboratory technique for measurement and calibration, *J. Geophys. Res.*, **102**, 14,899–14,913.
- Salisbury, J. W., and A. Wald (1992), The role of volume scattering in reducing spectral contrast of restrahten bands in spectra of powdered minerals, *Icarus*, **96**, 121–128.
- Stakes, D. S., and P. Schiffman (1999), Hydrothermal alteration within the basement of the sedimented ridge environment of Middle Valley, northern Juan de Fuca Ridge, *Geol. Soc. Am. Bull.*, **3**, 1294–1314.
- Taylor, L. A., A. Patchen, D. H. S. Taylor, and J. G. Chambers (1996), X-ray digital imaging and petrography of lunar mare soils: Data input for remote sensing applications, *Icarus*, **124**, 500–512.
- Thomson, J. L., and J. W. Salisbury (1993), The mid-infrared reflectance of mineral mixtures (7–14  $\mu\text{m}$ ), *Remote Sens. Environ.*, **45**, 1–13.
- Wänke, H., and G. Dreibus (1988), Chemical composition and accretion history of terrestrial planets, *Philos. Trans. R. Soc. London, Ser. A*, **325**, 545–557.
- Whyte, F. (1966), Dumbarton Rock, *Scot. J. Geol.*, **2**, 107–121.
- Wyatt, M. B., and H. Y. McSween Jr. (2002), Spectral evidence for weathered basalt as an alternative to andesite in the northern lowlands of Mars, *Nature*, **417**, 263–266.
- Wyatt, M. B., V. E. Hamilton, H. Y. McSween Jr., P. R. Christensen, and L. A. Taylor (2001), Analysis of terrestrial and Martian volcanic compositions using thermal emission spectroscopy: 1. Determination of mineralogy, chemistry, and classification strategies, *J. Geophys. Res.*, **106**, 14,711–14,732.

---

P. R. Christensen, Department of Geological Sciences, Arizona State University, Tempe, AZ 85287, USA.

V. E. Hamilton, Hawaii Institute of Geophysics and Planetology, University of Hawaii at Manoa, Honolulu, HI 96822, USA.

H. Y. McSween Jr., K. A. Milam, and J. M. Moersch, Planetary Geosciences Institute, Department of Earth and Planetary Sciences, University of Tennessee, 306 Geological Sciences Building, Knoxville, TN 37996-1410, USA. (kmilam@utk.edu)